Journal of Materials Processing Technology 225 (2015) 19–23

Journal of Materials Processing Technology

journal homepage: www.elsevier.com/locate/jmatprotec

Quantitative characterization of porosity and determination of elastic modulus for sintered micro-silver joints

James Carr[a,*], Xavier Milhet[b], Pascal Gadaud[b], Severine A.E. Boyer[b], George E. Thompson[a], Peter Lee[a]

[a] School of Materials, The University of Manchester, Manchester M13 9PL, UK
[b] Institut Pprime, UPR CNRS 3346, Dept. Physics and Mechanics of Materials, ENSMA – Université de Poitiers, 1 Avenue Clément Ader, Téléport 2, 86961 Futuroscope – Chasseneuil, France

ARTICLE INFO

Article history:
Received 9 January 2015
Received in revised form 24 March 2015
Accepted 25 March 2015
Available online 21 May 2015

Keywords:
Sintered joint
Electron microscopy
Tomography
Finite element method
Microstructural evolution
Micromechanics

ABSTRACT

High resolution serial block-face scanning electron microscopy has been performed on sintered micro-silver pastes that are used as lead replacement joints for die bonding. The size and spatial distributions of the porosity before and after ageing were determined by quantification of the segmented 3D images. The elastic modulus was determined by an image-based finite element model and validated by results obtained from a dynamical resonance method. In agreement with contemporary analytical models on the elastic behaviour of porous materials, the elastic modulus was found to be a function of pore fraction only. Ageing the specimens does not alter the density or Young's modulus.

1. Introduction

Sintered micro-silver pastes are good candidates to replace lead-based alloys for die bonding of power electronics due to their excellent electrical properties and high melting temperature as described by Li et al. (2013) who investigated the creep properties of these materials. Other mechanical properties of sintered micro-silver pastes can be found in the literature where Siow (2012) has provided a review of the work done in determining elastic modulus, strength and factors affecting the bonding strength of such joints. However, very few give a relationship between mechanical properties and porosity. Furthermore, no work has been done on the impact of ageing the material. With respect to the elastic behaviour, Panin et al. (2005) concluded that an increase in grain size due to annealing had no effect on the elastic properties as determined by nano-indentation.

Lifetime prediction of the entire system requires quantifying the evolution of the porous structure during thermal ageing in order to understand the modification of mechanical properties dominated by the porous structure of the joint material. The effect of the pore distribution on the elastic properties of sintered micro-silver pastes during ageing is one of the key parameters for modelling the elastic behaviour of the entire electronic system in the operating conditions. This study represents a first step towards addressing this issue by using imaging to determine the porous structures of both as-sintered material and aged material and relating it to the elastic properties.

Several analytical models have been proposed that link porosity with the elastic moduli of porous materials. Mackenzie (1950) states that the Young's modulus, E, as a function of the pore fraction, P, is of the form

$$E = E_0(1 - aP + bP^2) \quad (1)$$

where E_0 is the Young's modulus of the solid material and a & b depend on the shape of the pores, although the exact form of this dependence is unknown. The work of Ashby et al. (2000) on foams takes into account how E scales with P:

$$E = cE_0(1 - P)^n \quad (2)$$

where $0.1 \leq c \leq 4$ and $n \approx 2$.

Ramakrishnan and Arunachalam (1990) provided a model consistent with Eq. (2), but further demonstrated that it is possible to predict the Young's modulus of a porous solid as a function of pore

* Corresponding author at: HMXIF, Materials Science Centre, The University of Manchester, M13 9PL, UK. Tel.: +44 0161 306 2250.
E-mail address: james.carr@manchester.ac.uk (J. Carr).

http://dx.doi.org/10.1016/j.jmatprotec.2015.03.037

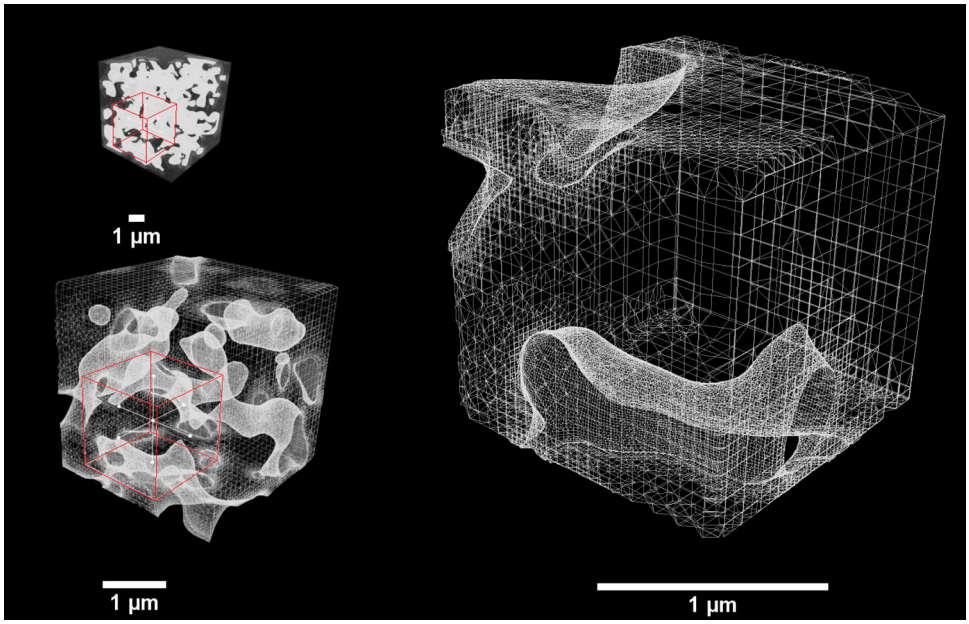

Fig. 1. A wire-frame display of the mesh produced by snappyHexMesh at increasingly higher magnifications to illustrate the refinement of the mesh.

fraction knowing only the Young's modulus and Poisson ratio of the solid material, i.e. E_0 and ν_0 respectively, by

$$c = \frac{1}{1 + (2 - 3\nu_0)P} \tag{3}$$

where ν_0 is the Poisson ratio of the solid material. Ramakrishnan and Arunachalam (1990) verified this analytical model using idealized 2D finite element (FE) models.

Following advancements in computing power, synthetic 3D FE meshes based on statistical models of porous solids were simulated. Roberts and Garboczi (2000) used such an approach to model the elasticity of porous ceramics and showed their results to be consistent with the analytical model proposed by Bert (1985) who developed another empirical model that is very close in form to Eq. (2) for spherical pore geometries. Advancements in 3D imaging have allowed the replacement of such synthetic meshes with real image-based meshes, which fully describe the complicated geometry of porous solids. Knackstedt et al. (2006) and Hardin and Beckermann (2007) used image-based 3D FE models of foams obtained by X-ray tomography (XRT) and used the analytical model proposed by Bert (1985) to fit their results.

Serial block-face scanning electron microscopy (SBFSEM) is a relatively new, destructive, high resolution 3D imaging technique, first used in a materials science context by Zankel et al. (2009), that is capable of achieving significantly higher spatial resolutions compared with XRT. The authors use SBFSEM datasets to produce FE models of the sintered pastes that are validated against experimentally determined values for Young's modulus using a dynamic resonance method (DRM) as described by Gadaud et al. (2009) who derived a formalism for interpreting the torsional vibrations to determine elastic and shear moduli.

2. Materials and methods

Heraeus LTS 043 04P2® Ag paste was sintered using an alternative processing route as described by Caccuri et al. (2014), which includes a final sintering step at 240 °C for 3 min under 10 MPa. This allows production of the bulk specimen with the same microstructure as the real joint material. Ageing was performed at 125 °C for 1500 h in air. The density of the specimens prior to and after ageing was obtained from the weight to volume ratio using a high precision Sartorius MZ1 balance (accuracy better than 10 mg) and a micrometer (accuracy better than 1 µm).

Sectioning for the SBFSEM was performed at a nominal thickness of 75 nm, and an accelerating voltage of 2 kV in high vacuum mode was used to obtain backscattered electron micrographs of the block-face in the SEM. Magnification settings on the SEM give a pixel size of 37.5 nm.

Pore fractions were obtained from the segmented binary image. The quantification of size and spatial distributions considers pores unconnected to the large singular porous network. Images were segmented by an automatic thresholding algorithm developed by Otsu (1979) who used image histograms to determine threshold values for the segmentation. Volumes and barycentres were calculated following connected component labelling as described by Suzuki et al. (2003) using a 6 voxel neighbourhood. A clustering ratio is defined as the ratio of the expected nearest neighbour distance given a random distribution with the measured mean nearest neighbour distance. Chandrasekhar (1943) provides a derivation of the mean nearest neighbour distance for a distribution of random particles.

Segmented sub-volumes of the tomographic datasets acquired from the SBFSEM data were used to produce FE models such that each sub-volume provides a single datapoint for the pore fraction and corresponding Young's modulus. This is achieved by forming a stereolithography surface at the pore/matrix interface of the binarized image and utilizing the 'snappyHexMesh' utility bundled with OpenFOAM. A refinement level of 5 was used to produce a volume mesh of the matrix composed of hexahedra and split hexahedra as shown in Fig. 1. For the boundary conditions, a uniform stress of 10 Pa was applied normally to the face of the mesh and the adjacent face was kept at a fixed displacement. Known physical parameters for pure silver (density: 10.490 g cm^{-3}, Poisson ratio: 0.37 & Young's modulus: 83 GPa) were used in the simulation. The simulation was run using the 'solidDisplacementFoam' solver bundled with OpenFOAM; convergence criteria were set such that the global residual does not exceed 10^{-10}. The Young's modulus was obtained from the simulation by using the known applied stress and the calculated global strain, determined by the average displacement field of the pressurized face.

3. Results and discussion

3.1. Quantification

Fig. 2 shows a 2D comparison of the pore distribution of the same sample immediately after sintering (Fig. 2a) and after ageing (Fig. 2b). A clear evolution of the microstructure was observed; the pores after sintering are homogeneously distributed while, after ageing, the pores are relatively heterogeneous and the pore size has increased substantially. Some areas of the aged material were almost free of pores, whereas other areas displayed large pores. However, while measurements in two dimensions (2D) give an insight of the pore microstructure evolution upon ageing, a three dimensional (3D) study is valuable in giving the actual pore spatial distribution, shape and size as well as the pore connectivity, and the evolution of these quantities. An example of such differences between quantification of porosity for 2D and 3D studies is presented by Chaijaruwanich et al. (2007) who use XRT.

Since 3D experiments using SBFSEM are destructive, two different specimens, with densities as close as possible to the as-sintered state, $7.8 \pm 0.2\,g\,cm^{-3}$ and $8.0 \pm 0.2\,g\,cm^{-3}$ respectively, were used to investigate the 3D evolution of the pore distribution. It is noted that, after direct measurement of weight and sample dimensions before and after ageing, the density of the material was found to remain constant, i.e. close to $8\,g\,cm^{-3}$ in this case. Reconstructed volumes are displayed in Fig. 3, where the silver matrix has been made transparent and only the porosity is visible. Initial quantification of the depth profile of the pore density, as revealed in Fig. 4, shows a root mean square (RMS) deviation of 1% implying a high level of homogeneity in the density as a function of depth for the as-sintered solder. In comparison, the aged solder was found to have an increase in RMS deviation by a factor of 2.4. Additionally, Fourier transforms of the depth profiles revealed a dominance in the lower spatial frequency domain. As observed qualitatively for the 2D analysis in Fig. 2, the quantification of the pore spatial distribution in 3D was less homogeneous after ageing than in the as-sintered state.

Both the size distributions (Fig. 4b) of the image volumes and the spatial distributions (Fig. 4c) of the pore clusters show a positive shift and an increase in frequency of the mid-sized pores leading to a higher mean value. Clustering ratios also reveal a move from an approximately random distribution (0.9629) of pore clusters to a more clustered distribution (0.8773).

A reduction in the number of pore clusters, in addition to their spatial and size distributions, is indicative of an agglomeration of pores that provides larger clusters with more distant nearest neighbours. In other words, ageing tends to favour the disappearance of the smaller pores by either agglomeration or growth, leading to an increase of the average pore size, a shift of the distribution towards larger sizes and a larger distance between the nearest neighbours.

A further interesting feature stands in the evolution of the sphericity. While it has been estimated to be close to 0.7 just after sintering, it evolved towards 1 after ageing. All these factors tend to account for the surface energy reduction to be the main driving force for pore evolution during ageing. This may be helped by vacancy diffusion along the material grain boundaries.

3.2. Influence on the elastic properties

The dramatic evolution of the porosity during ageing may substantially alter the elastic properties of sintered micro-silver pastes since certain regions exhibit a high level of porosity while others are almost pore free. Upon ageing, the material structure tends to become heterogeneous and the local load bearing surface may vary substantially.

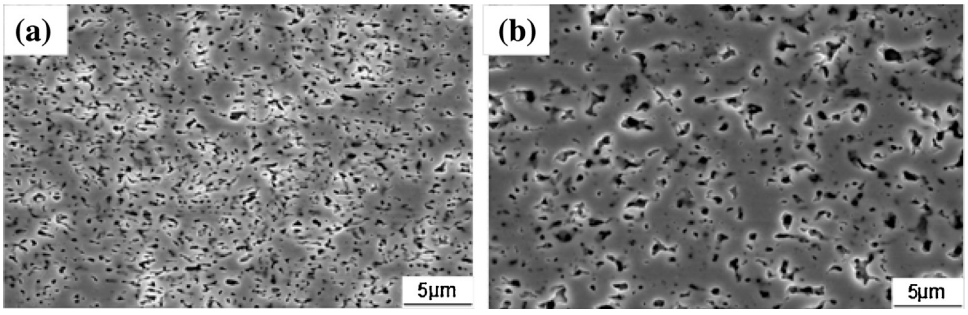

Fig. 2. Scanning electron micrographs of the polished surface, highlighting the evolution of the porosity from the as-sintered specimen (a) to the aged specimen (b).

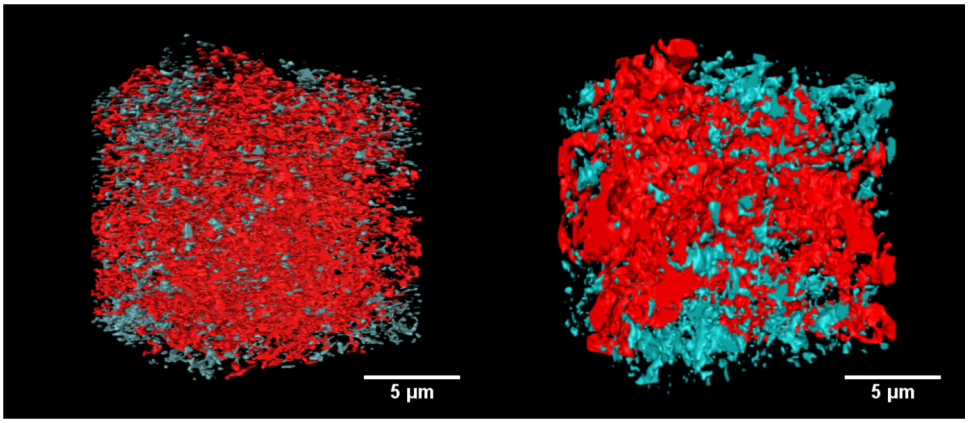

Fig. 3. Surface meshes of the reconstructed porosity for the as-sintered (left) and aged (right) solders. A single pore network shown in red was observed in both samples. Pore clusters shown in blue are quantified in isolation to observe size and spatial distributions of the unconnected porosity and its subsequent impact on performance. (For interpretation of reference to color in this figure legend, the reader is referred to the web version of this article.)

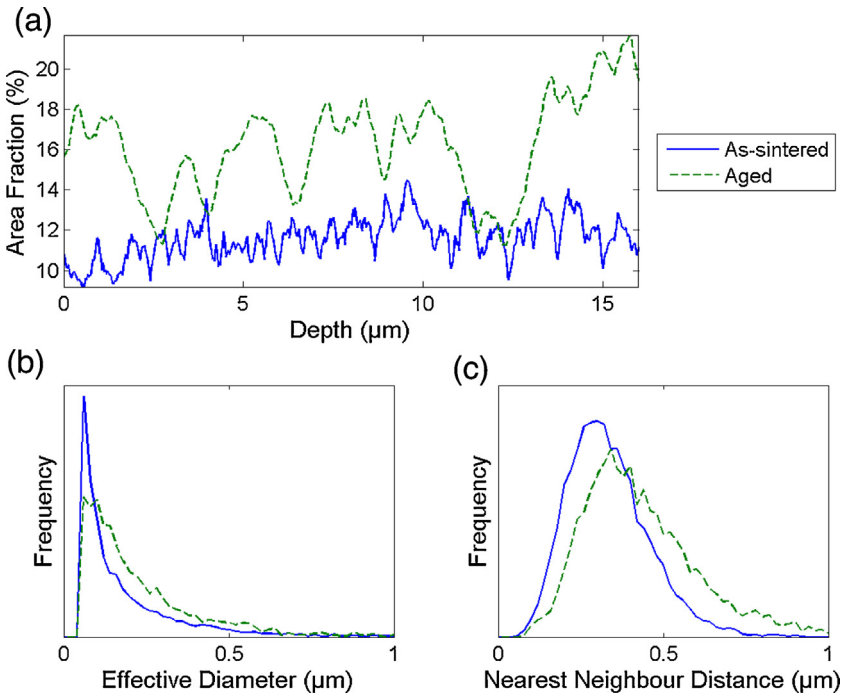

Fig. 4. (a) The pore area fraction as a function of depth from the segmented volume; (b) the effective diameter distribution. The mean effective diameter is 95 nm for the as-sintered sample and 140 nm for the aged sample. Frequency is normalized with pore number density; (c) the nearest neighbour distributions. For the as-sintered and aged samples respectively, the mean nearest neighbour distances are 289 nm and 366 nm, and the clustering ratios are 0.9629 and 0.8773. The frequency is normalized with pore number density.

The Young's modulus as a function of the pore density has been modelled using the reconstructed 3D images. Validation of the model has been achieved by comparison with experimentally determined data.

Owing to the high convergence criteria specified in Section 2, solutions for the displacement fields in the produced FE meshes converged for a total of 7 of 10 attempted cases. Example cases are shown in Fig. 5 for both the as-sintered and aged specimens. These renderings, in contrast to Fig. 3, display the silver matrix as solid and the porosity as transparent. Qualitatively, it is plain to see a larger displacement field associated with the aged specimen across the face, indicating a reduced elastic performance. It is also apparent that the maximum displacements occur around porous regions, thus indicating that the local plastic performance is a function of the distribution of the porosity in agreement with Surappa et al. (1986) who observed strong plastic deformation in the vicinity of macro-porosity for Al–7Si–0.3Mg alloy.

Comparing the values for Young's modulus with the quantified pore fraction (i.e. specimen density) agrees closely with the proposed empirical model by Ramakrishnan and Arunachalam (1990). This model has been validated using DRM experimental measurements on as-sintered materials obtained with various sintering loads, i.e. as-sintered specimens with a large spectrum of densities. As displayed in Fig. 6, the Young's modulus predicted by the model is not a function of the pore distribution and geometry. The Young's modulus is, to a good approximation, only a function of the material density and is not altered or modified by ageing globally. Locally, however, significant variation in the porous structure is observed in the aged samples. The reduced elasticity in regions of high porosity is, therefore, a likely candidate for sites of initial failure of the sintered joint. The size and curvature of the porosity are also important for the fatigue properties of the material as concluded by Yi et al. (2003) where large pores were found to be exclusively responsible for crack initiation. The amount of porosity was also found to

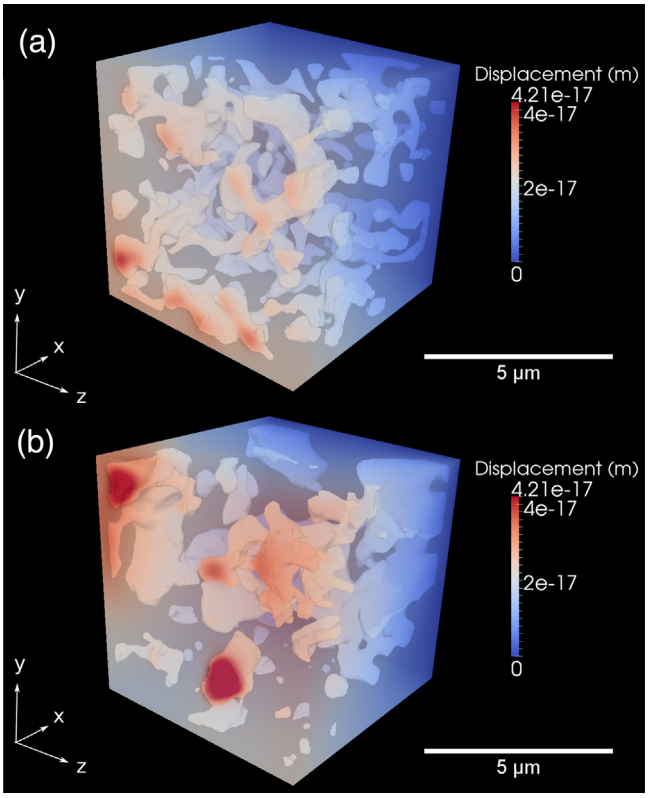

Fig. 5. Surface rendered volume meshes extracted from the larger datasets depicted in Fig. 3. These show the solution of the displacement field within sub-volumes of the (a) as-sintered and (b) aged specimens. Stress was applied along the positive x direction.

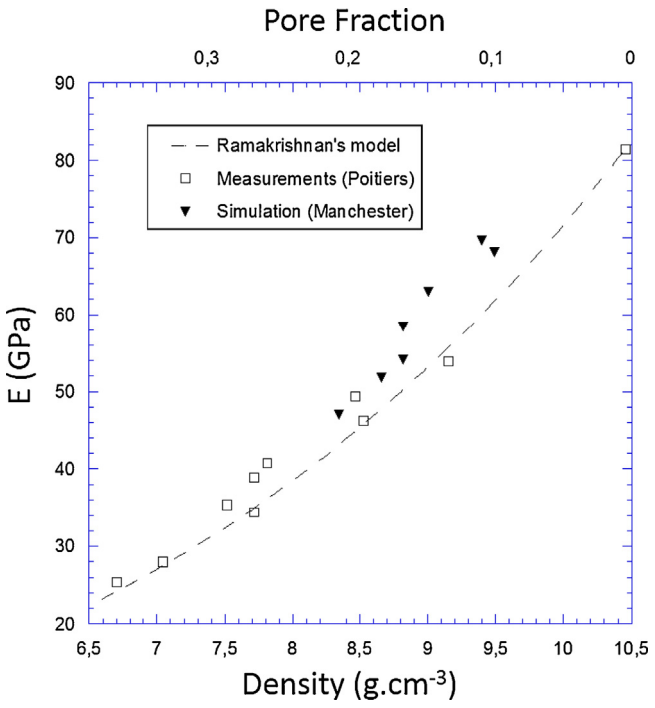

Fig. 6. A combination of results for both the FE modelling and direct elasticity measurements plotting Young's modulus against pore fraction. The fit shows an agreement of the data with the proposed empirical model.

correlate with fatigue life although this has not been evaluated in the case of sintered micro-silver joints. It is anticipated that these regions also significantly impact the plastic behaviour of the material. Work is currently ongoing to evaluate a failure model, which incorporates both the plastic and elastic behaviour during ageing.

4. Conclusions

- Sintered micro-silver pastes have been successfully imaged in high resolution 3D to observe the evolution of the porous networks during ageing.
- Quantification of the size and distribution of the porous networks is consistent with Ostwald ripening.
- The model proposed by Ramakrishnan and Arunachalam (1990) has been validated for silver foams of porosity ≤20%, implying that the elastic properties are only a function of density. This is consistent with the implications of both Mackenzie (1950) and Ashby et al. (2000).
- The porosity became increasingly heterogeneous after ageing, and the local variation of pore fraction corresponds to a local variation of the elastic behaviour.
- Global density variations were not appreciable during ageing, implying a constant value for elasticity over time. This is consistent with Panin et al.'s conclusions that the global elastic behaviour is unaffected by annealing.
- The results produced here are an initial step towards complete micromechanical modelling of the full system such that ideal processing specifications can be determined.

Acknowledgements

The authors are very grateful to Michel Gerland & Vincenzo Caccuri (Institut Pprime UPR 3346 CNRS) and Teruo Hashimoto (University of Manchester) for the specimen production and image acquisition. We acknowledge the EPSRC for funding of the LATEST 2 Programme Grant, and the Research Complex at Harwell which is partly funded by the EPSRC (EP/102249X/1). The work has received the financial support from the ANR (Agence Nationale de la Recherche) – FIDEA. The authors are grateful to Dr. Le Henaff, IMS, Bordeaux – France, for his help during sintering of the materials.

References

Ashby, M., Evans, A., Fleck, N., Gibson, L., Hutchinson, J., Wadley, H., 2000. Metal Foams. Elsevier, http://dx.doi.org/10.1016/B978-075067219-1/50006-4
Bert, C.W., 1985. Prediction of elastic moduli of solids with oriented porosity. J. Mater. Sci. 20, 2220–2224, doi:10.1007/BF01112307.
Caccuri, V., Milhet, X., Gadaud, P., Bertheau, D., Gerland, M., 2014. Mechanical properties of sintered Ag as a new material for die bonding: influence of the density. J. Electron. Mater. 43, 4510–4514, http://dx.doi.org/10.1007/s11664-014-3458-x
Chaijaruwanich, A., Lee, P., Dashwood, R., Youssef, Y., Nagaumi, H., 2007. Evolution of pore morphology and distribution during the homogenization of direct chill cast AlMg alloys. Acta Mater. 55, 285–293, http://dx.doi.org/10.1016/j.actamat.2006.08.023
Chandrasekhar, S., 1943. Stochastic problems in physics and astronomy. Rev. Modern Phys. 15, 1–89, http://dx.doi.org/10.1103/RevModPhys.15.1
Gadaud, P., Milhet, X., Pautrot, S., 2009. Bulk and coated materials shear modulus determination by means of torsional resonant method. Mater. Sci. Engine: A 521, 303–306, http://dx.doi.org/10.1016/j.msea.2008.09.115
Hardin, R.A., Beckermann, C., 2007. Effect of Porosity on the Stiffness of Cast Steel. Metall. Mater. Trans. A 38, 2992–3006, http://dx.doi.org/10.1007/s11661-007-9390-4
Knackstedt, M.A., Arns, C.H., Saadatfar, M., Senden, T.J., Limaye, A., Sakellariou, A., Sheppard, A.P., Sok, R.M., Schrof, W., Steininger, H., 2006. Elastic and transport properties of cellular solids derived from three-dimensional tomographic images. In: Proc. R. Soc. A: Math. Phys. Eng. Sci, pp. 2833–3286, http://dx.doi.org/10.1098/rspa.2006.1657
Li, X., Chen, G., Wang, L., Mei, Y.H., Chen, X., Lu, G.Q., 2013. Creep properties of low-temperature sintered nano-silver lap shear joints. Mater. Sci. Eng.: A 579, 108–113, http://dx.doi.org/10.1016/j.msea.2013.05.001
Mackenzie, J.K., 1950. The elastic constants of a solid containing spherical holes. Proc. Phys. Soc. Sect. B 63, 2–11, http://dx.doi.org/10.1088/0370-1301/63/1/302
Otsu, N., 1979. A threshold selection method from gray-level histograms., http://dx.doi.org/10.1109/TSMC.1979.4310076
Panin, A.V., Shugurov, A.R., Oskomov, K.V., 2005. Mechanical properties of thin Ag films on a silicon substrate studied using the nanoindentation technique. Phys. Solid State 47, 2055–2059, http://dx.doi.org/10.1134/1.2131144
Ramakrishnan, N., Arunachalam, V.S., 1990. Effective elastic moduli of porous solids. J. Mater. Sci. 25, 3930–3937, http://dx.doi.org/10.1007/BF00582462
Roberts, A.P., Garboczi, E.J., 2000. Elastic properties of model porous ceramics. J. Am. Ceram. Soc. 83, 3041–3048, http://dx.doi.org/10.1111/j.1151-2916.2000.tb01680.x
Siow, K.S., 2012. Mechanical properties of nano-silver joints as die attach materials. J. Alloys Compds. 514, 6–19, http://dx.doi.org/10.1016/j.jallcom.2011.10.092
Surappa, M., Blank, E., Jaquet, J., 1986. Effect of macro-porosity on the strength and ductility of cast Al–7Si–0.3Mg alloy. Scripta Metall. 20, 1281–1286, http://dx.doi.org/10.1016/0036-9748(86)90049-9
Suzuki, K., Horiba, I., Sugie, N., 2003. Linear-time connected-component labeling based on sequential local operations. Comp. Vision Image Understanding 89, 1–23, http://dx.doi.org/10.1016/S1077-3142(02)00030-9
Yi, J.Z., Gao, Y.X., Lee, P.D., Flower, H.M., Lindley, T.C., 2003. Scatter in fatigue life due to effects of porosity in cast A356-T6 aluminum–silicon alloys. Metall. Mater. Trans. A 34, 1879–1890, http://dx.doi.org/10.1007/s11661-003-0153-6
Zankel, A., Kraus, B., Poelt, P., Schaffer, M., Ingolic, E., 2009. Ultramicrotomy in the ESEM, a versatile method for materials and life sciences. J. Microsc. 233, 140–148, http://dx.doi.org/10.1111/j.1365-2818.2008.03104.x.